Coupling of lattice Boltzmann shallow water model with lattice Boltzmann free-surface model

Yann Thorimbert[1,*], Jonas Lätt[1], Bastien Chopard[1]

Department of Computer Science, University of Geneva, Carouge, 1227, Switzerland

Abstract

We present a scheme for coupling a 2D lattice Boltzmann free-surface solver with a 1D lattice Boltzmann shallow water solver, allowing to save computational effort and efficiently realize multiscale systems. The accuracy of the coupling is validated with two tests. First, we compare the numerical and analytical solutions in a setup with fixed inflow current and outflow water level in a canal. Secondly, the physics of wave propagation and reflection in a domain is investigated in a coupled simulation, and compared to the solutions obtained in both a pure free-surface and a pure shallow-water simulation. Finally, a performance test is carried out to demonstrate that the overhead of the coupling is negligible. A quantitative validation of this type of coupling for the lattice Boltzmann method is novel, and opens the door to a range of large-scale simulations of canals and other hydrodynamic systems.

Keywords: lattice Boltzmann, free-surface, shallow water, two-phase flows, validation

1. Introduction

The lattice Boltzmann (LB) method is now recognized as a successful numerical solver for the incompressible Navier-Stokes equations (NSE). The method is based on the Boltzmann equation (see [1, 2] for more details on the method), and it is therefore sufficiently general to simulate a wide set of physical systems, including multi-phase and free-surface flows. Free-surface

*Corresponding author

Email address: yann.thorimbert@unige.ch (Yann Thorimbert)

[1]Department of Computer Science, University of Geneva

and shallow water models are commonly used to simulate, among others, rivers and coastal flows. The work of [3] demonstrates the ability of shallow water models to simulate erosion with high performance, while [4] uses them to study sediment transport. An application of a shallow water model to marine flow in coastal areas can also be found in [5]. Free-surface flows can be computed with good efficiency in the LB method using a Volume-of-Fluid (VOF) approach [6]. Such an approach is for instance used in [7] for the simulation of sediment transport in rivers. This paper highlights the limits of the VOF approach from a computational perspective, as it shows the inability to simulate a river segment significantly longer than 10 km even using a parallel computer with several hundred CPU cores.

A VOF free-surface model was used in [8] for simulating an Oscillating Water Column wave energy conversion device, and a similar approach using the LB method was studied in our previous work [9]. While a free-surface model allows us to fully simulate a 3D flow, an approach based on the shallow water equation saves computational cost, allowing to simulate much larger domains. Shallow water models may also be considered as a solution to overcome spurious energy dissipation (see [9]) occurring over long distances in underresolved LB VOF simulations. As a downside, the shallow water equation is based on more limiting physical assumptions (see Section 2.1 below) than the free-surface approach. A coupling between a LB shallow water model and a LB free-surface model therefore offers a way to obtain the best of both worlds, using a free-surface model to simulate the fluid on small portions of the domain requiring high accuracy and with complex flow patterns, while pure wave or flow propagation and reflection phenomena are simulated on larger portions with a shallow water model.

The purpose of this article is to present a scheme for coupling a LB free-surface model with a LB shallow water model. To illustrate this coupling and assess its quality, we consider here the 2D-1D case. The coupling accuracy is studied here through two different tests, the former focusing on flow rate transmission between coupled lattices, while the latter focuses on wave propagation. The aim of such a coupling is to save computational time thanks to the shallow water model while preserving accuracy allowed by the free-surface model. As a result of the lower dimensionality of the shallow water model, its computational cost (see section 5) is one order of magnitude lower than the one of the free-surface model; this particular point is crucial since one can expect this computational scale difference to be reflected in the time and space scale of the corresponding simulated domains, giving the

opportunity to simulate multiscale systems.

We present the LB, free-surface LB VOF and LB shallow water methods in the second section. In the third section, we describe the scheme used to couple shallow water and free-surface systems. The coupling model is tested in the fourth section, where different benchmarks are used. Performance considerations are given in the last section.

2. Lattice Boltzmann method

The fundamental principles of the LB method (see [2, 10, 11] for more details) originate from statistical mechanics. The Boltzmann equation describes the statistical kinetics of gas molecules [12]. As a consequence, the quantity solved for in this method is the particle distribution function, and the macroscopic variables such as velocity or pressure are derived quantities, defined as velocity moments of the distribution function. The method is Cartesian mesh based, allowing fast mesh generation, and the method is inherently parallelizable and scalable [13] thanks to spatial locality of its interaction pattern.

The lattice Boltzmann equation is obtained by truncating the continuum Boltzmann equation in velocity space [14, 15]. A number of q particle distributions, also named populations, is attached to each lattice site. These populations can be seen as the discrete counterpart of the particle distribution function in the continuous Boltzmann equation. The q velocities $\mathbf{c_i}$ of the lattice correspond to the Gaussian quadrature points used to resolve integrals in the discrete velocity space. The population representing the statistics of particles entering the lattice site $\mathbf{r}$ at time t with velocity $\mathbf{c_i}$ is denoted by $f_i(\mathbf{r}, t)$. The number of discrete velocities used in the numerical scheme determines the connectivity of lattice nodes with their neighbors. One uses the notation "DdQq", where d is the number of dimensions and q the number of velocities, to denominate the chosen scheme. For instance, a D1Q3 lattice has been used in the present study to run the shallow water simulations.

The collision term of the Boltzmann equation is often approximated by the Bhatnagar-Gross-Krook (BGK) collision model [16], which uses a single relaxation time. In this model, the time evolution is expressed through the relation

$$f_i(\mathbf{r} + \Delta t \mathbf{c_i}, t + \Delta t) - f_i(\mathbf{r}, t) = -\frac{1}{\tau} \left(f_i(\mathbf{r}, t) - f_i^{eq}(\mathbf{r}, t) \right), \qquad (1)$$

where f_i^{eq} are the equilibrium populations, Δx and Δt are the discrete space and time steps respectively, and τ is the relaxation parameter. The equilibrium populations f_i^{eq} are obtained as a finite expansion of the Maxwell-Boltzmann equilibrium distribution, up to second order with respect to the Mach number.

The macroscopic density and velocity can be computed from the populations as:

$$\rho = \sum f_i, \qquad \rho \mathbf{u} = \sum \mathbf{c_i} f_i. \tag{2}$$

A Chapman-Enskog analysis (see [15] for instance) demonstrates that the above scheme is asymptotically equivalent to solutions of the incompressible Navier-Stokes equations, in the limit of small Mach number.

In the present study, 2D VOF simulations are run using an approach of large-eddy simulation (LES), based on a Smagorinsky subgrid-scale model([17, 11, 10]). Although the flow is expected to be laminar in coupling interface regions, it can become turbulent in any other part of the domain.

2.1. LB Shallow Water model

An early attempt to solve the shallow water equations using the LB method can be found in [18]. The LB shallow water model used in this study follows the line of [19]. As in [20], we consider a 1D flow in a rectangular channel with slope I and width B. The shallow water equations, also named Saint-Venant equations in 1D, are derived from mass and momentum Navier-Stokes equations, assuming that the water depth is very small as compared to the characteristic length of flow structures. Further assumptions include fluid incompressibility, a hydrostatic pressure profile, negligible viscosity effects, and a small value of the slope I. Under these assumptions, the Navier-Stokes equations are reduced to the following relations:

$$\frac{\partial h}{\partial t} + \frac{\partial (hu)}{\partial x} = 0, \tag{3}$$

$$\frac{\partial (hu)}{\partial t} + \frac{\partial (gh^2/2 + hu^2)}{\partial x} = gh(I - J), \tag{4}$$

where h denotes the water height from the bottom to the surface, u is the depth-averaged horizontal velocity, g is the gravitational acceleration, and J a term accounting for the friction force due to channel bottom. The latter term is modeled as [21]:

$$J = n^2 u^2 \left(\frac{2h + B}{hB} \right)^{4/3}, \tag{5}$$

where n is the Manning coefficient of the canal.

In the LB model for simulating shallow water equations, the water height h is assimilated to the first-order velocity moment ρ ("the density"), and is computed as the sum of the populations. In this study we use the D1Q3 model presented in [20]. One can show that, for Froude number $Fr = u/\sqrt{gH}$ close to 1, spurious viscous contribution appears in this model [20], thus constraining the type of regime simulated.

2.2. LB free-surface VOF model

The free-surface model considers two-phase fluid compounds with a large density ratio, akin to water-air systems in normal atmospheric conditions. It simulates the physics of the heavy fluid only, and replaces the effect of the light fluid onto the heavy one through a condition of zero parallel shear stress along two-phase interface. In the LB VOF approach, additionally to the usual fluid variables, every cell keeps trace of the local mass m and volume fraction VF. While $VF = 1$ on bulk cells of the heavy fluid, it is related to the fluid density on interface cells: $VF = m/\rho$. Thus, the cells of the fluid mesh are split into three categories: "fluid cells" (cells completely occupied by the heavy fluid) in which $VF = 1$, "empty cells" (cells completely occupied by the light fluid) with $VF = 0$, and "interface cells" on which the volume fraction is comprised between 0 and 1. The interface layer between fluid and empty cells is always closed, so that an empty cell is never in the neighboring of a fluid cell.

At each iteration, the progression of the two-phase interface is simulated through a mass advection process, and the cell types are updated accordingly. For an interface cell, the population f_I^{out} that is streamed from an empty cell in the direction i is given by $f_I^{out} = f_i^{eq} + f_I^{eq} - f_i$, where I denotes the direction opposite to i. The equilibrium populations here are computed using a constant reference air density, set to 1 in our model.

Classical bounce-back conditions [22] are applied to wall cells, in the same way as in standard single-phase simulations. A more detailed presentation of VOF free-surface models and their LB implementation can be found in [23, 24]. Note that even if the solution of the flow field is obtained via a LB approach, the advection equation for the VOF fill level can be solved in

different ways, as for instance in [25], where it is discretized with a finite volume method.

2.3. Other works on SW-FS coupling

To the best of the authors' knowledge, there exist only few studies regarding the coupling of shallow water and free-surface (SW-FS) models. A coupling between a 3D free-surface solver and a 1D shallow water solver, both based on finite differences method, is studied in [26]. The numerical scheme is validated through the study of the flow in a curved channel, with an oscillatory inflow velocity condition and imposed outflow. The study is however limited, as it does not represent effects of friction along the channel bed, and the water depth is constant along the channel. At the coupling interface, the water level in the 1D simulation is imposed as the average of the water level of the 3D simulation, while the velocity in the 1D simulation is used as the value to impose in all the corresponding 3D sites. Within this setup, a good match for the time evolution of the free-surface height is found between the coupled system and a single 3D free-surface simulation. A coupling between a 3D LB VOF free-surface solver and a 2D LB shallow water solver is also presented in [27]. Since this publication is targeted at a computer visualization community, it does not include any quantitative validation of the coupling.

In [28, 29], a distinction is made between coupling strategies involving systems that are dimensionally homogeneous and physically heterogeneous, and systems that are dimensionally heterogeneous and physically homogenous. Applications with different coupled shallow water models are depicted. The present work, however, involves both dimensionally heterogeneous and physically heterogeneous systems. A study of different coupling types such as via source terms, boundary conditions or state variables, is also found in [30] and is applied to shallow water systems.

3. Coupling scheme

In a coupled simulation, we use free-surface and shallow water lattices to represent different parts of the physical domain. At the connection between the two domains, an overlap region is used, in which the two lattices are superimposed. At both ends of this overlap region, a coupling between the lattices is performed. In this way, the coupling is not performed at the same

location on both lattices, in order to avoid amplification of errors and resulting numerical instabilities. Figure 1 depicts the configuration. Note that, in a similar way as done in [27] for the 3D-2D case, the coupling interfaces at coordinates $x = B$ and $x = C$ are vertical columns with a thickness of 1 cell in the x direction. The overlap zone has a length of $C - B$ cells.

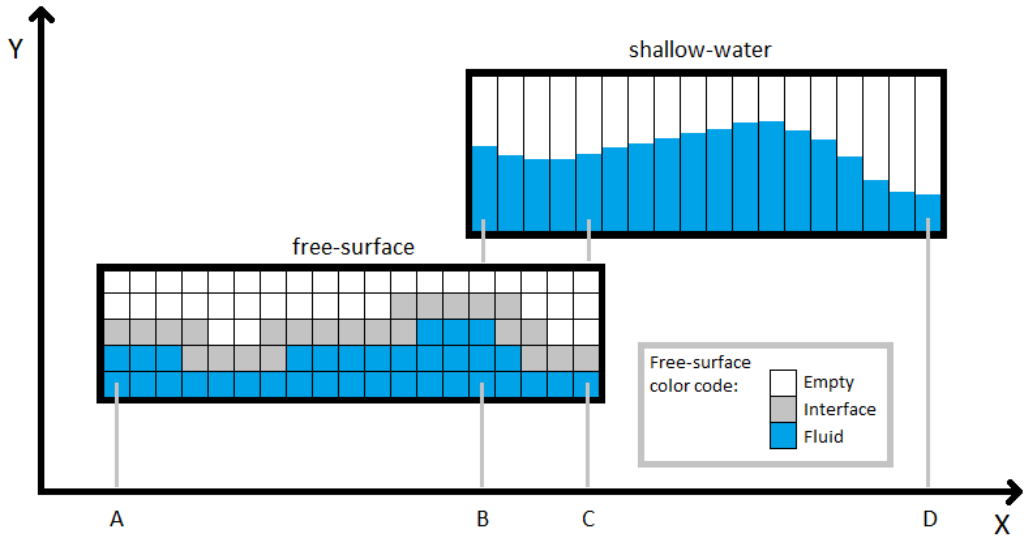

Figure 1: Configuration of the lattices and their coupling. The area below the curved line in the free-surface lattice represents the VF value of interface cells, while the height simulated in the shallow water lattice is represented by a discrete water column.

In the coupling scheme presented below, lattices are synchronously updated. This implies that, at the coupling interface only, data from one of the lattices has to be saved in temporary variables before the coupling scheme is applied.

3.1. Coupling from shallow water to free-surface

At the coordinate $x = C$, the coupling acts as a boundary condition for the free-surface lattice, which imposes a water height and velocity determined by the shallow water flow, incoming from the right. The following steps are performed each iteration:

First step.. Update the free-surface cell types according to the shallow water height. In order to perform this step, the volume fraction VF of the free-surface lattice is computed according to the water height h of the shallow

water lattice on the same interface cell. The volume fraction of a corresponding, superimposed interface free-surface cell is $h - \lfloor h \rfloor$. The y coordinate of this cell is $\lfloor h \cdot \Delta x \rfloor$.

Second step.. The horizontal velocity is obtained from the shallow water lattice at the same interface location $x = C$. This value is used as a basis for the velocity to impose at each cell of the fluid column of the free-surface lattice. Here, missing information for the horizontal velocity along depth $u(y)$ has to be completed. Three types of distribution have been tested: a constant velocity profile, a quadratic velocity profile and a logarithmic velocity profile. In the first case, one imposes the same velocity to each cell along the depth. For the quadratic case, the imposed velocity profile corresponds to a steady-state solution of a laminar free-surface flow, with a constant current Q and a constant fluid height H. Figure 2 displays an example of a quadratic profile. As indicated in [31] for instance, the expected velocity profile is parabolic in a theoretical laminar free-surface flow. The parabolic profile is characterized by the following three parameters: the mean velocity $\bar{u} \equiv Q/S$, where S is the cross section of the domain, and the velocity at the bottom and at the level of the free surface, $u(0)$ and $u(H)$ respectively. These values depend on the properties of the walls. The latter two conditions, combined with the flow condition $1/H \int_0^H u(y)dy = \bar{u}$, yield a unique velocity profile. In our case, we apply a no slip condition at the bottom, $u(0) = 0$. Since the free-surface model assumes zero parallel shear stresses at the interface, the maximum theoretical velocity is reached at the surface $y = H$, and the theoretical velocity profile reads:

$$u(y) = \frac{3\bar{u}y}{H}\left(1 - \frac{y}{2H}\right). \tag{6}$$

The maximum velocity value $3\bar{u}/2$ is in theory obtained at $y = H$. However, real laminar flows in a canal show a slight velocity decrease near the water surface, due to the so-called dip effect [32] that arises in canals with finite width due to friction forces, as well as non-zero parallel shear stress at the interface. These phenomena are not implemented in our study. Also, our free-surface model is two-dimensional and we assume there are no lateral walls. An example of the velocity profile for laminar flow in the free-surface model is shown in Figure 2.

In summary, as we couple the velocity from the shallow water to the free-surface lattice at $x = C$, we apply the theoretical velocity profile to the water column, as provided by Equation 6, with mean velocity $\bar{u} = u_{SW}$ and

a water height $H = h_{SW}$. These values are imposed to free-surface cells as Zou-He velocity boundary conditions [33], even for the last, interface cell of the column (both the free-surface completion scheme and Zou-He completion scheme are involved at the top cell, the latter using the value from the former if needed). When the water height changes, the populations of the new interface cell are initialized at equilibrium.

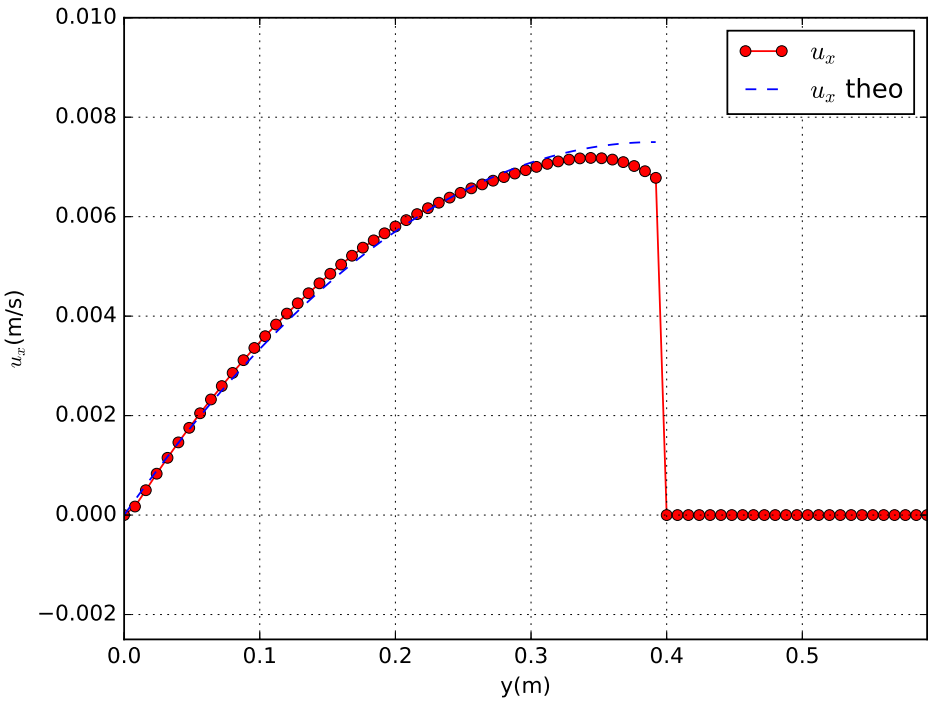

Figure 2: Velocity profile along the water height y from the bottom $y = 0$ to the free surface $y = 0.4$ m, obtained from a free-surface simulation with constant inlet and outlet flows. In this example, $\Delta x = 8 \cdot 10^{-3}$ m and $\Delta t = 8 \cdot 10^{-5}$ s.

In turbulent flows, the velocity profile is known to take a logarithmic form [34]. This profile has been tested and we show in Section 4.2.1 that, for the benchmarks used, the difference in the results is not significantly impacted by the choice of the velocity profile. In the canal test cases (see Section 4.1), the use of either quadratic or logarithmic velocity profile improved the overall accuracy of the result by approximately 5%, while in the wave propagation tests (see Section 4.2), the improvement of accuracy amounted to approxi-

mately 2.5%. In this article, the quadratic profile was used unless otherwise specified.

We would like to point out that, if the main phenomenon of interest is the propagation of surface gravity waves, an alternative velocity profile could be considered. In this case, if the properties (e.g. period and amplitude) of the waves created during the simulation are known, one can deduce the pressure and velocity distributions under the water surface. The profile for these quantities is expressed in terms of the amplitude, the period, and the water depth [34], and could be directly imposed at the coupling interface. However, the determination of wave properties, and in particular their period, is non trivial, and an additional numerical effort would be required to compute their time-varying properties.

As a final comment, the y-component of the velocity cannot be directly obtained from the shallow water lattice. However, we deduce it, at a first-order approximation, by keeping track of the h values on interface cells from the previous iterations. The value $(h_t - h_{t-1})/\Delta t$ is then taken as an approximation of the vertical component of the velocity, and is uniformly distributed over the depth. Higher order schemes may be considered, but we have not investigated them presently, and this study includes only the above one.

3.2. Coupling from free-surface to shallow water

At the position $x = B$, the coupling acts as a boundary condition for the cell of the shallow water lattice, using flow properties of the free-surface lattice arriving from the left.

The water height of a free-surface column at coordinate x can be computed as:

$$h_{FS} = \Delta x \sum_{y=0}^{H} \mathrm{VF}(x, y). \tag{7}$$

The mean horizontal velocity u_{FS} of the free-surface lattice is similarly computed as an average over a water column. These values are imposed to the shallow water lattice on interface cell, by setting the populations to $f_i = f_i^{eq}(h_{FS}, u_{FS}) + f_i^{neq}(h_{SW}, u_{SW})$. The non-equilibrium part is preserved as it does not change the evaluation of macroscopic height and velocity. The value of the non-equilibrium part can be computed as indicated in [20]:

$$f_0^{neq} = \tau \Delta t \left[\left(1 - \frac{gh}{v^2} - 3\frac{u^2}{v^2} \right) \partial_x (hu) + 2 \left(\frac{u^2}{v^2} - \frac{gh}{v^2} \right) u \partial_x h \right], \tag{8}$$

and $f_1^{neq} = f_2^{neq} = -f_0^{neq}/2$. The spatial derivatives of h and u are evaluated through a second order centered scheme.

3.3. Coupling parameters

The numerical parameters that can be freely chosen in our model are the length of the overlap zone and the time and space steps Δt and Δx. In this paper, the latter two parameters are equal in the free-surface and the shallow water simulation. Although it is in principle wasteful to apply the same time step in both simulations whereas the free-surface model often requires a finer time step, this choice remains appropriate in our case, in which the computational effort is largely dominated by the free-surface simulations (see Section 5), while the computations of the shallow water lattice are negligible.

The stability of the simulations is affected by the size of the overlaping zone. For the benchmarks studied, an overlap zone of 0.2 m was found to be a good value in terms of stability. One can see the overlap zone as a buffer area allowing to make a relaxation of the coupling variables going from one lattice to the other one. When the size is too small, the spurious quantities are increased by the feedback between lattices. This behaviour was expected, since the physics of each lattice are of different nature, in addition to the inhomogeneity of lattice topology. Hence, the coupling here is substantially different from that involved in a grid refinement scheme for instance, which allows for smaller interaction stencils.

Another parameter of the simulation is the relaxation time τ, which relates to the fluid viscosity. We have kept this parameter free, and its influence on the accuracy is presented in the results below.

It should be pointed out that, for our coupled system to produce meaningful results, one should make sure that physical phenomena occurring near the coupling interface are properly captured by both the free-surface and the shallow water model. It is reminded that the assumptions of the shallow water model are valid only if the horizontal characteristic scale (*e.g.* the wavelength of a wave) is much larger than the vertical scale (*e.g.* water depth). In the case of surface wave propagation in a canal of depth H, waves in the shallow water system propagate with velocity $v = \sqrt{gH}$, while in the free-surface system waves travel with velocity $v = \sqrt{g\lambda \tanh(2\pi H/\lambda)/(2\pi)}$, assuming their behavior obey linear wave theory (see [34] for instance), with λ the wavelength. Since $\tanh(x) \approx x$ for small values of x, these expressions tend to be equivalent for small values of H/λ.

We conclude this section by remarking that height, velocity, or any physical quantity, are defined twice in overlapping areas, by both the free-surface and the shallow water lattices. Since there is no *a priori* reason to choose the value from one lattice rather than from the other one, we choose here to define any quantity q of the fluid in the overlap area through linear interpolation as $q(x) = \alpha \cdot q_{SW}(x) + (1 - \alpha) \cdot q_{FS}(x)$, where $\alpha = (x - B)/(C - B)$. While this choice has an impact on the visualization of the flow quantities, it does not affect the results of either the free-surface or the shallow water simulation, as the physical variables of the overlap zone are not explicitly used in the coupling scheme.

4. Results

4.1. Benchmark

Our benchmark case is similar to the one of [20]. It imposes an inflow current Q_0 and an outflow water height h_L on a canal of given length L, as depicted in Figure 3, and in this way allows us to test the coupling in both ways (from free-surface to shallow water and vice versa). This benchmark

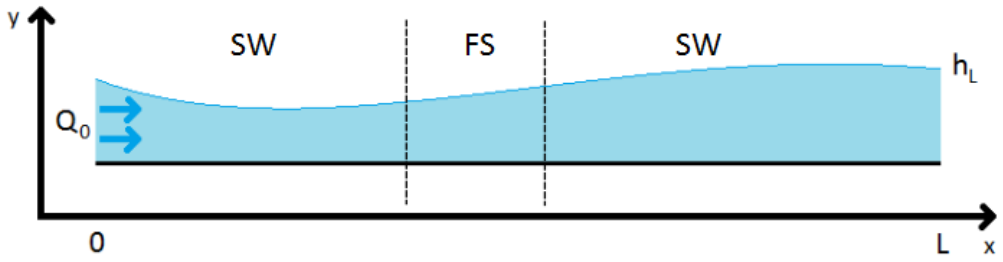

Figure 3: Configuration of the benchmark test with a canal of length L. The inflow current Q_0 and the outflow water height h_L are imposed. The free-surface lattice is in the center of the domain and is surrounded by longer, shallow water lattices.

tests the response of both height and velocity to perturbations, and is motivated by its similarity with potential real-life applications to irrigation canals [20, 35]. The simulation domain is decomposed into three parts: two shallow water parts and one free-surface part in the center. A bounce-back condition is applied at the bottom of the free-surface part. The inflow current and outflow height are imposed to the shallow water lattices in the same way as in [20], by completing the unique missing population. The shallow water differential equation corresponding to the discussed condition reads:

$$\frac{\partial h}{\partial x} = \frac{gh(I-J)}{gh-u^2}, \tag{9}$$

where $u = Q_0/(Bh)$, with the condition $h(L) = h_L$, and

$$J = \frac{n^2 Q_0^2}{B^2 h^2 \left(\frac{Bh}{B+2h}\right)^{4/3}}. \tag{10}$$

An approximated solution for this equation is obtained numerically using a solver for ordinary differential equations based on Runge-Kutta method.

The results are validated by computing the mean relative error of the data from the coupling model to the reference solution h_{ref} of Equation (9). We define the mean relative error ϵ as:

$$\epsilon = \frac{1}{N}\sum_{i=0}^{N} \frac{\mid h(i\Delta x) - h_{ref}(i\Delta x) \mid}{h_{ref}(i\Delta x)}, \tag{11}$$

where $N \equiv L/\Delta x$ is the total number of cells along x-axis. All three domains are included in the calculation of the error. The parameters used for the simulations are $\Delta x = 8 \cdot 10^{-3}$ m, $\Delta t = 8 \cdot 10^{-5}$ s, $H_0 = 0.4$ m, $\tau_{SW} = 0.51$, $L = 4$ m, $I = 2.6 \cdot 10^{-3}$, $B = 0.1$ m, $n = 0.0103$ and $g = 9.81$ m/s^2. The length of the full free-surface domain is 0.8 m and the length of each overlap zone is 0.2 m.

For a given set of values for the quantities described above, the resulting flow reads:

$$Q_i = \sqrt{I}\frac{BH}{n}\left(\frac{BH}{B+2H}\right)^{2/3}. \tag{12}$$

The above value of Q_i is used for the initial condition of the flow velocity $u_i = Q_i/(BH)$ everywhere in the domain. In an initial stage of the simulation, the flow is linearly increased up to $Q_0 = 1.5 \cdot Q_i$, as done in [20]. The Froude and Reynolds number corresponding to the described setup are $Fr \approx 0.5$, $Re \approx 10^6$ respectively. The water level is initialized at a value $h(x) = H_0$ everywhere in the domain.

The proposed benchmark is highly demanding for our coupling model. Indeed, the LB, VOF-based free-surface model suffers from energy dissipation over long distances, and is therefore poorly adapted to a simulation of a long canal. As pointed out in the introduction, this is precisely one of the

reasons why a SW-FS coupling model is needed in situations where both long-range wave propagation and a precise representation of the flow structure are required in different parts of the simulation domain.

Figure 4 shows the evolution of ϵ as a function of time for $\tau_{FS} = 0.55$, $\tau_{FS} = 0.53$ and $\tau_{FS} = 0.501$, and the solution from the shallow water model alone. An installation wave and its reflections perturb the simulation at the beginning, due to the initial flow increase from Q_i to Q_0. At time $t \approx 10$ s, a steady state is reached. Figure 6 shows that the mean relative error linearly decreases with the lattice spacing Δx, for a given set of relaxation times for the free-surface and shallow water lattices. The simulations show that the accuracy of the results linearly decreases as the value of τ_{FS} departs from 0.5, as shown in Figure 5. To explain this, we point out that the considered benchmark case assumes an inviscid flow, and that the shallow water equation similarly solves the non-viscous shallow water equations. Note that it has been shown in [20] that even the LB shallow water model exhibits a non-null viscosity, that does not correspond to the one of the free-surface model. Therefore, a residual error is found, although the free-surface domain yields best results at low viscosity, when τ is close to 0.5. Figure 7 compares the elevation profile at time $T = 29.7$ s in the theoretical case and in the coupled simulation: discrepancies of less than 5% appear on the form of an offset in the inlet side of the domain. As a result, the total mass of fluid slightly differs from the initial one; this effect is quantified in Section 4.3.

4.2. Wave transmission

In the next numerical test, we focus on the transmission of waves from the shallow water to the free-surface simulation and vice versa, by tracking the evolution of surface elevation along time. For this reason, we use a symmetric test case in which the water elevation is initialized with the following profile:

$$h(x) = H_0 + H_{drop} \cdot \mathrm{e}^{-(x-X_0)^2/\left(2\sigma^2\right)}. \tag{13}$$

For the results presented below, the parameters are $H_0 = 0.195$ m, $H_{drop} = 0.1$ m, $X_0 = 2$ m and $\sigma = 0.15$ m. The total length of the domain is 4 m while the length of the central, free-surface domain is 1 m and overlap areas of 0.2 m. The corresponding Froude and Reynolds numbers are $Fr \approx 0.2$, $Re \approx 10^5$ respectively. We refer to this test under the term of "Gaussian drop", due to the similarity of its behaviour with the waves generated by a droplet falling into water. The symmetry of the system, the reflections of

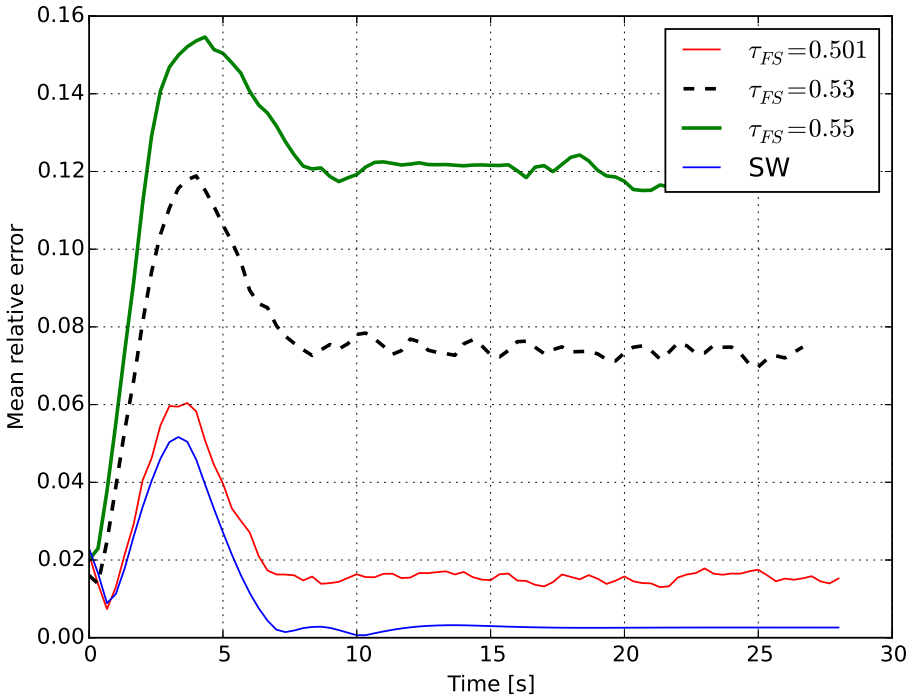

Figure 4: Evolution of mean relative error ϵ as a function of time, for three different values of τ_{FS} with SW-FS model and shallow water model.

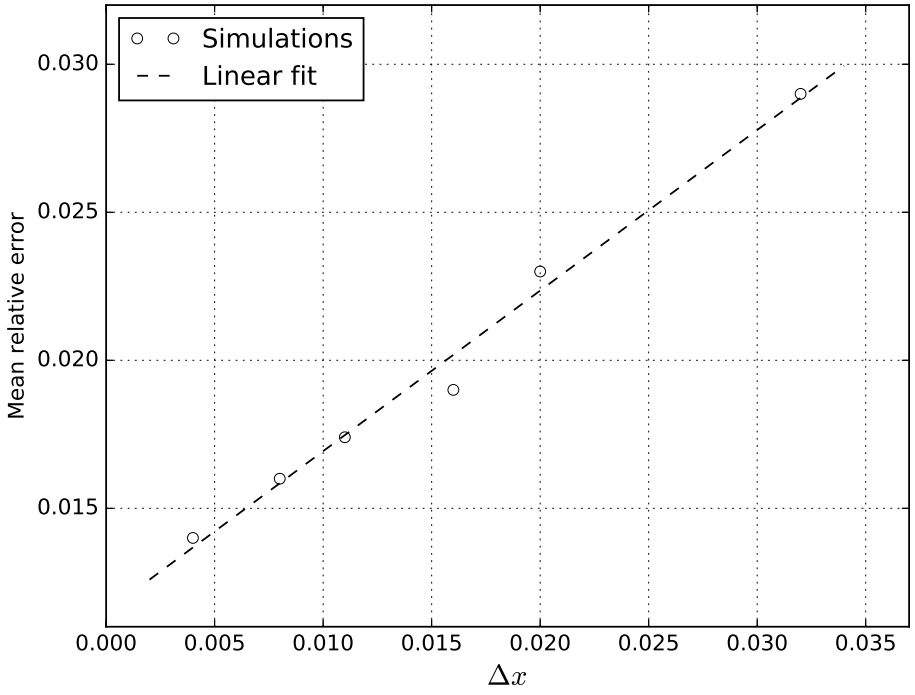

Figure 5: Mean relative error in the steady state as a function of lattice spacing Δx for constant $\tau_{SW} = 0.51$ and $\tau_{FS} = 0.501$. The dotted line corresponds to a linear fit.

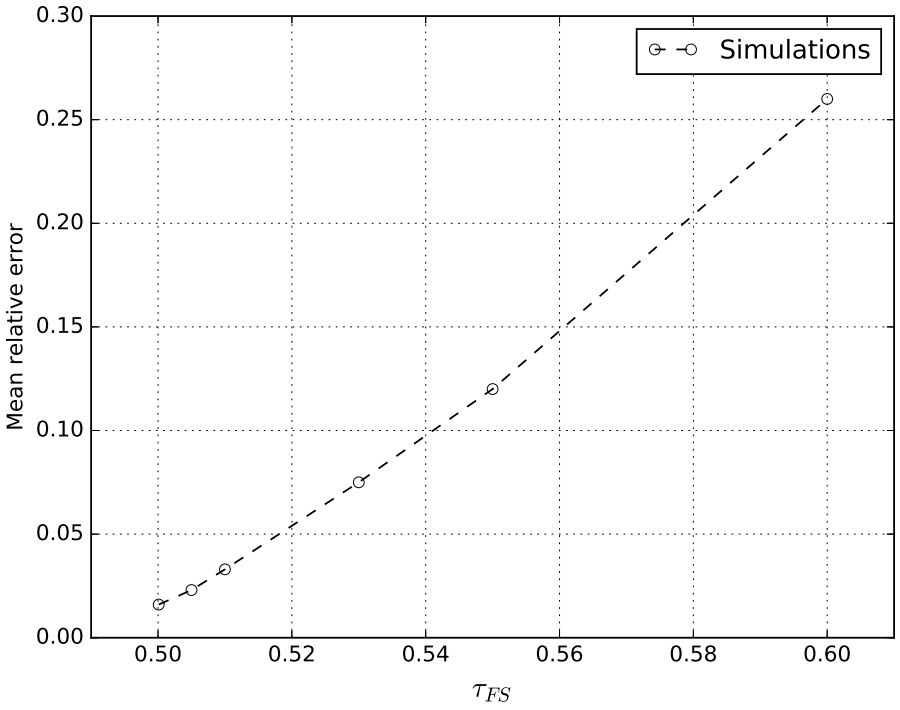

Figure 6: Mean relative error as a function of τ_{FS} for constant $\tau_{SW} = 0.51$, in the steady state.

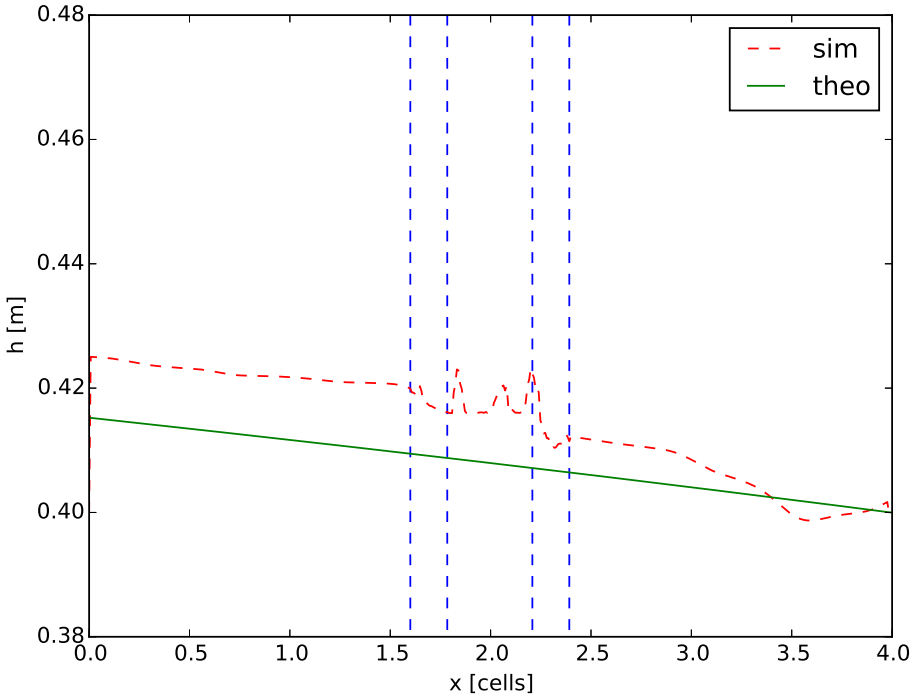

Figure 7: Water elevation along the channel for the simulation using the coupling scheme (red dotted line) and in the theoretical case (green line), at time $T = 29.7$ s. Overlap areas are delimited by vertical dotted lines.

waves on boundary walls and the resulting superimposition of waves makes it relevant for the study of wave propagation. It allows us to verify wave properties over a long time while keeping the simulation domain small.

4.2.1. Velocity profile in free-surface model

As discussed in Section 3.1, the shape of the velocity profile requires an *ad-hoc* choice to be made, given that the data from the shallow water lattice is one-dimensional. Figure 8 shows the difference of water elevation at different time steps for the Gaussian drop, for results obtained from constant, quadratic and logarithmic velocity profiles. In the Gaussian drop test case as well as in the canal test, the mean relative difference between the results for different profiles is less than 2.5%. Apart from the observation that, in our benchmark, the actual velocity profile appears to be much less important than the total flow, another possible reason for this small difference is that, even starting from a constant velocity profile along depth, the profile adapts after on the x-axis, as shown in Figure 9. Thus, a constant profile has a small impact on the mean relative error for a steady flow; however, it has an influence on the capacity of the coupling scheme to react to quick flow changes, as in the canal benchmark test. For this reason, the quadratic profile was preferred.

4.2.2. Comparison between models

Figure 10 compares the solutions obtained with the shallow water model, the free-surface model, and the coupled system respectively for the Gaussian drop.

Figure 11 shows the mean relative deviation of the shallow water solution, as compared to the coupled and the pure free-surface solutions. It can be observed that the difference between coupled system and pure shallow water method is essentially equal to the difference between coupled system and pure free-surface. Regardless if one chooses free-surface or shallow water as reference solutions, the mean relative error remains smaller than approximately 3% throughout the simulation, which is consistent with the mean relative error found in the previous benchmark.

4.3. Mass conservation

As discussed above, information has to be reduced/augmented when passing from one lattice to the other, because the two involved models are 1D or 2D respectively. This transformed information impacts the macroscopic

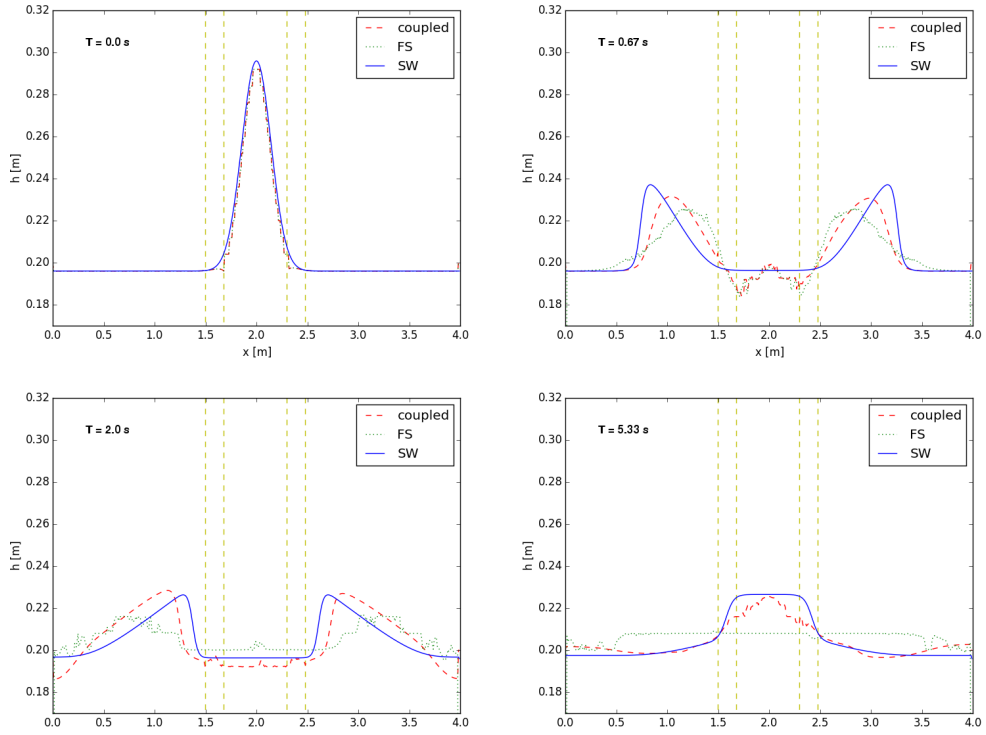

Figure 8: Comparison of the solution obtained for the Gaussian drop test with constant, quadratic and logarithmic velocity profiles at different time steps.

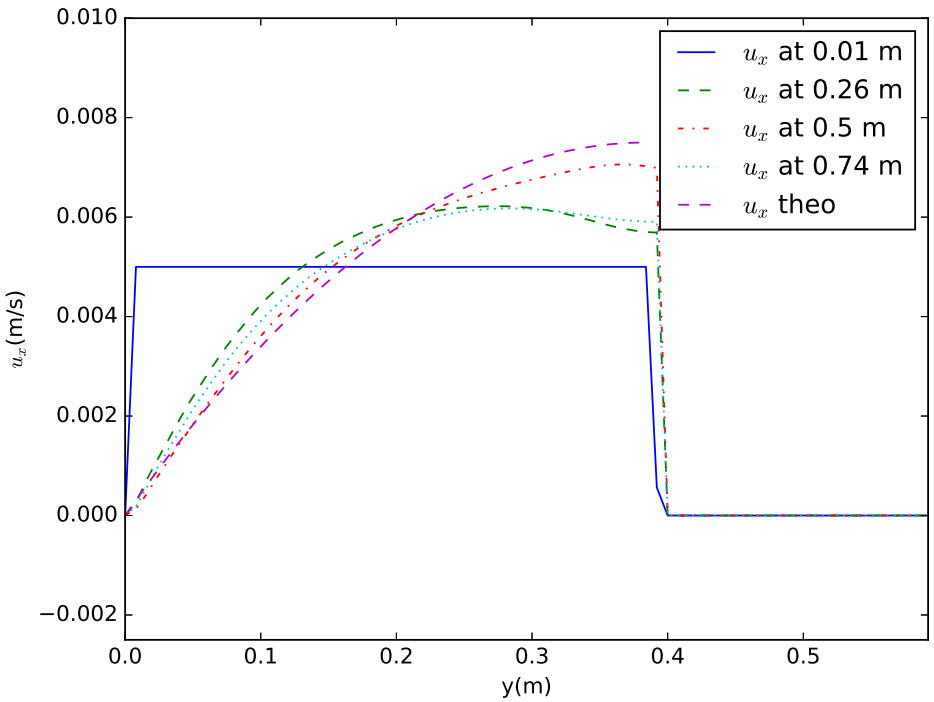

Figure 9: Example of velocity profile along y-axis at different locations on the x-axis, after 0.5 s of simulation ($5 \cdot 10^3$ iterations). In this test a constant velocity (continuous line) is imposed at $x = 0$ in the free-surface lattice, and there is no shallow water lattice. A parabolic distribution is recovered for the velocity after a short distance.

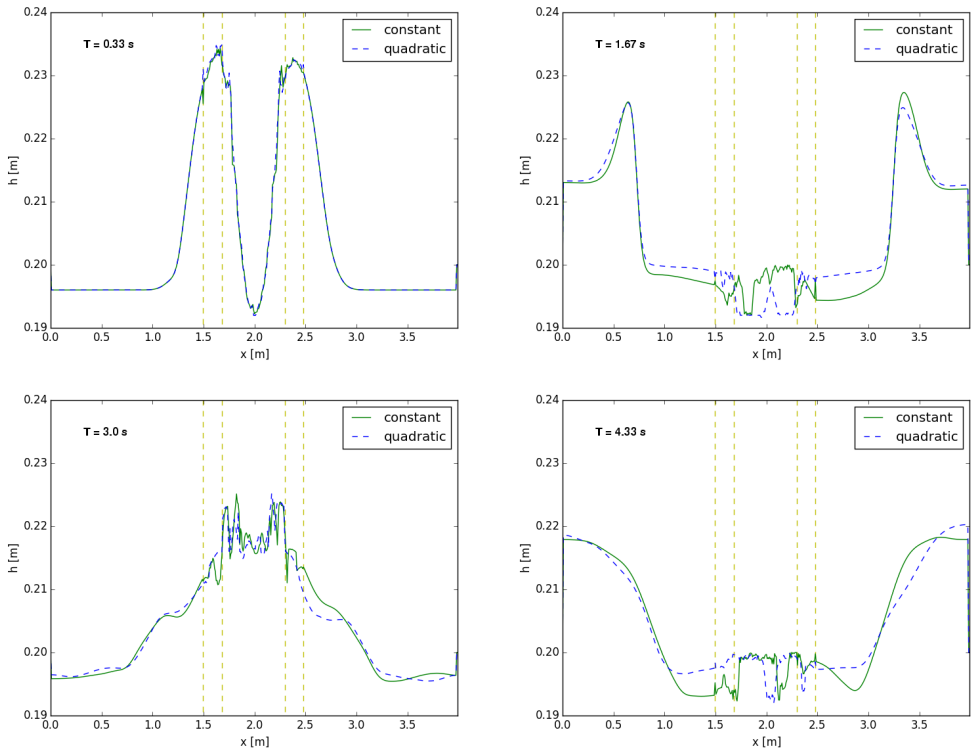

Figure 10: Solutions obtained from shallow water model only, free-surface model only, and coupled model for the Gaussian drop. The physical time T is indicated in each case. Vertical dashed lines delimit overlap areas between lattices.

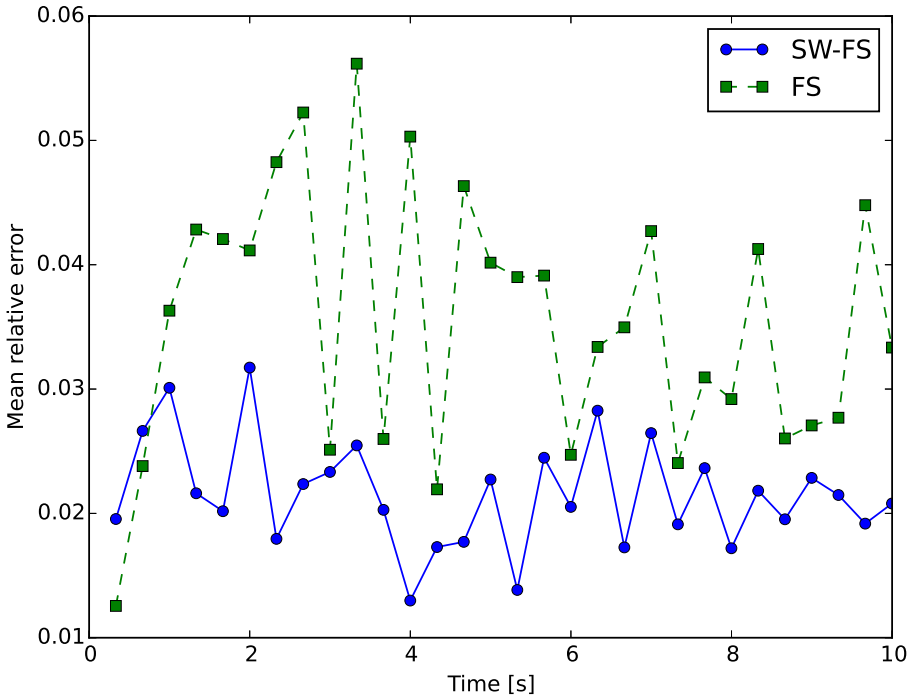

Figure 11: Mean relative deviation of the coupled (SW-FS) and free-surface model compared to the shallow water solution, in the case of the Gaussian drop test.

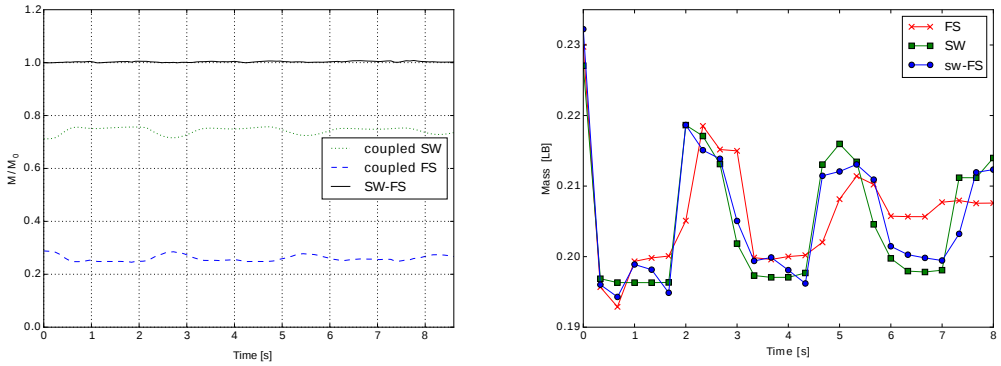

Figure 12: (left) Total mass of fluid during a simulation for the Gaussian drop test. Continuous line shows the total (SW + FS) fluid mass M divided by the initial mass M_0. The dotted and dashed lines show the repartition of fluid mass into shallow-water and free-surface parts respectively. (right) Total mass of fluid contained inside the overlap zone for three distinct simulations: pure SW, pure FS and SW-FS systems.

variables on the two lattices through the boundary conditions on the coupling interfaces (see Sections 3.1 and 3.2 above). For this reason, one can expect mass conservation to be affected by the coupling scheme.

The left plot of figure 12 shows the fluid mass in the Gaussian drop simulation. Small variations of mass can be seen locally (less than 1% of the total fluid mass), but no systematic loss of mass occurs. We conclude that spurious mass gain or loss introduced by the coupling scheme is negligible. Simulations of pure shallow water, pure free-surface and coupled SW-FS systems have been performed in order to compare the evolution of the mass of fluid contained inside the overlap area (even though for pure systems no special treatment is applied in this area). This way, mass evolution at the SW-FS transition zone can be compared to pure systems. The right plot figure 12 shows that this difference is comparable to the error previously found for the water level in the same problem.

5. Performance

The free-surface model is computationally much more expensive than the shallow water model, mainly because of the representation of a 2D domain, as opposed to 1D in the shallow water case. Figure 13 illustrates the dependence of the total execution time on the relative length of the free-surface

domain, as a fraction of the total domain. Note that our code has not been optimized and simply follows the description of the coupling model given here. Thus, the performance results depicted below constitute an initial investigation, as the coupling overhead may reveal sensitive to the specific implementation used. Consistently with our expectations for the coupled model, the execution time is substantially reduced when a larger part of the domain is represented by the shallow water system. It is important to stress here that for sake of implementation simplicity, the shallow water lattice is in fact used over the whole domain, although its values outside the domain defined for shallow water simulations are ignored and never involved in computations of physical quantities. As one can deduce from this figure, it is not worthwhile using the coupled system if the domain fraction represented by the free-surface model is larger than about 75 %, as in this case the overhead due to the coupling algorithm weighs out the reduction of computational cost obtained by the shallow water scheme. This condition is not expected to cause any problems in practice, since the free-surface simulation is intended to be concentrated on areas of restricted size, with highly resolved local flow structures, while the shallow water model should be applied to areas of extended lengths ($L_{SW} >> \lambda$), where wave or current propagation is the central investigated phenomenon.

6. Conclusion

The proposed coupling scheme allows us to significantly reduce the computational time compared to a pure free-surface approach. Its accuracy is found to be satisfying both in the case of flows dominated by current transmission, as well as for flows dominated by wave transmission, as long as the flow conditions at the coupling interface satisfy the assumptions of the shallow water model.

Time interpolation should be considered in the future as a possible improvement of the current model, as well as an implicit scheme to solve the coupling interface and reduce the length of the overlap zone. Also, for the use in large scale simulations, a parallel implementation of our coupling scheme and its software implementation should be investigated. While both shallow water and free-surface models are proven to be efficiently parallelizable, the overhead of the coupling scheme could have a negative impact on the overall performance, or ability to achieve efficient load balancing.

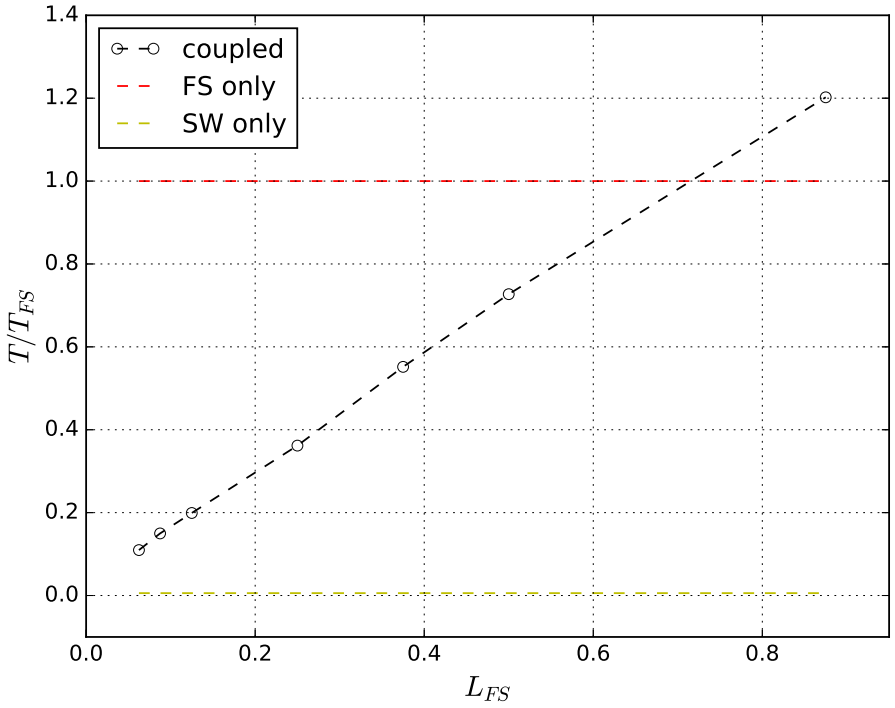

Figure 13: Ratio of execution time between coupled model pure free-surface, for different values of the fraction L_{FS} of the domain simulated by the free-surface model. As a rough observation, when less than 75 % of the domain is simulated by free-surface, the coupling scheme becomes worthwile in terms of performance. Note that in our software implementation, for simplicity, the shallow-water lattice covers the whole domain, though its values are ignored at locations where free-surface domain is defined.

A limitation of the model is that one should carefully ensure that the shallow water lattice always simulates flows with Froude number less than unity, since it yields spurious viscous terms in regimes with Fr close to 1 (see Section 2.1). Thus, regions with large Froude number, including transitions to these regions, must be simulated within the free-surface part of the domain.

Finally, a natural generalization of our numerical scheme will include its adaptation to a coupling between 1D or 2D shallow water and 3D free-surface. In this case, a proper velocity profile will need to be formulated, not only along the fluid height, but also in the transversal axis. The main ideas as developed here will apply.

[1] S. Succi, *The Lattice Boltzmann Equation, For Fluid Dynamics and Beyond*. Oxford University Press, 2001.

[2] S. Chen and G. Doolen, "Lattice Boltzmann methods for fluid flows," *Annu. Rev. Fluid Mech.*, vol. 30, p. 329, 1998.

[3] B. Benes, "Real-Time Erosion Using Shallow Water Simulation," in *Workshop in Virtual Reality Interactions and Physical Simulation "VRIPHYS" (2007)* (J. Dingliana and F. Ganovelli, eds.), The Eurographics Association, 2007.

[4] G. Simpson and S. Castelltort, "Coupled model of surface water flow, sediment transport and morphological evolution," *Computers & Geosciences*, vol. 32, no. 10, pp. 1600 – 1614, 2006.

[5] Y. Li, Y. Jin, Y. Yin, and H. Shen, "Simulation of shallow-water waves in coastal region for marine simulator," in *Proceedings of The 7th ACM SIGGRAPH International Conference on Virtual-Reality Continuum and Its Applications in Industry*, VRCAI '08, (New York, NY, USA), pp. 15:1–15:5, ACM, 2008.

[6] C. W. Hirt and B. D. Nichols, "Volume of fluid /VOF/ method for the dynamics of free boundaries," *Journal of Computational Physics*, vol. 39, pp. 201–225, Jan. 1981.

[7] A. Parmigiani, J. Latt, M. B. Belgacem, and B. Chopard, "A lattice Boltzmann simulation of the Rhone river," *Int. J. Mod. Phys. C*, vol. 24, no. 11, p. 1340008, 2013.

[8] I. Simonetti, L. Cappietti, H. E. Safti, and H. Oumeraci, "3D numerical modelling of oscillating water column wave energy conversion devices : current knowledge and OpenFOAM ® implementation," no. March 2016, pp. 497–504, 2015.

[9] Y. Thorimbert, J. Latt, L. Cappietti, and B. Chopard, "Virtual wave flume and oscillating water column modeled by lattice boltzmann method and comparison with experimental data," *International Journal of Marine Energy*, vol. 14, pp. 41 – 51, 2016.

[10] B. Chopard, P. Luthi, A. Masselot, and A. Dupuis, "Cellular automata and lattice boltzmann techniques: An approach to model and simulate

complex systems," *Advances in Complex Systems*, vol. 5, no. 2, pp. 103–246, 2002. http://cui.unige.ch/∼chopard/FTP/CA/acs.pdf.

[11] B. Chopard and M. Droz, *Cellular Automata Modeling of Physical Systems*. Cambridge University Press, 1998.

[12] S. Harris, *An Introduction to the Theory of the Boltzmann Equation*. Dover Publications, 1971.

[13] A. Peters, S. Melchionna, E. Kaxiras, J. Latt, J. Sircar, M. Bernaschi, M. Bison, and S. Succi, "Multiscale simulation of cardiovascular flows on the IBM Bluegene/P: Full heart-circulation system at red-blood cell resolution," in *Proceedings of the 2010 ACM/IEEE International Conference for High Performance Computing, Networking, Storage and Analysis*, SC '10, (Washington, DC, USA), pp. 1–10, IEEE Computer Society, 2010.

[14] X. He and L.-S. Luo, "Theory of the lattice Boltzmann method: From the Boltzmann equation to the lattice Boltzmann equation," *Physical Review E*, vol. 56, no. 6, pp. 6811–6817, 1997.

[15] P. J. Dellar, "Bulk and shear viscosities in lattice boltzmann equations," *Phys. Rev. E*, vol. 64, 2001.

[16] P. L. Bhatnagar, E. P. Gross, and M. Krook., "A model for collision processes in gases," *Phys. Rev.*, vol. 94, pp. 511–525, 1954.

[17] S. Hou, J. Sterling, S. Chen, and G. Doolen, "A lattice boltzmann subgrid model for high reynolds number flows," *Fields Institute Communications*, vol. 6, pp. 151–166, 1996.

[18] R. Salmon, "The lattice boltzmann method as a basis for ocean circulation modeling," *Journal of Marine Research*, vol. 57, no. 3, pp. 503–535, 1999.

[19] J. Zhou, "A lattice boltzmann model for the shallow water equations," *Computer Methods in Applied Mechanics and Engineering*, vol. 191, no. 32, pp. 3527 – 3539, 2002.

[20] P. van Thang, B. Chopard, L. Lefèvre, D. A. Ondo, and E. Mendes, "Study of the 1D lattice Boltzmann shallow water equation and its

coupling to build a canal network," *Journal of Computational Physics*, vol. 229, no. 19, pp. 7373–7400, 2010.

[21] W. Graf and M. Altinakar, *Hydraulique fluviale: écoulement et phénomènes de transport dans les canaux à géométrie simple*. Traité de Génie Civil, Presses polytechniques et universitaires romandes, 2000.

[22] X. He, Q. Zou, L. Luo, and M. Dembo, "Analytic solutions of simple flows and analysis of nonslip boundary conditions for the lattice boltzmann bgk model," *Journal of Statistical Physics*, vol. 87, pp. 115–136, 1997.

[23] C. Korner, M. Thies, T. Hofmann, N. Thürey, and U. Rüde, "Lattice boltzmann model for free surface flow for modeling foaming," *Journal of Statistical Physics*, vol. 121, no. 1-2, pp. 179–196, 2005.

[24] N. Thürey and U. Rüde, "Stable free surface flows with the lattice boltzmann method on adaptively coarsened grids," *Computing and Visualization in Science*, vol. 12, no. 5, pp. 247–263, 2009.

[25] C. F. Janssen, S. T. Grilli, and M. Krafczyk, "On enhanced non-linear free surface flow simulations with a hybrid lbm–vof model," *Computers and Mathematics with Applications*, vol. 65, no. 2, pp. 211 – 229, 2013. Special Issue on Mesoscopic Methods in Engineering and Science (ICMMES-2010, Edmonton, Canada).

[26] M. P. Daou, E. Blayo, A. Rousseau, O. Bertrand, T. Pigeonnat, C. Coulet, and N. Goutal, "Coupling 3D Navier-Stokes and 1D shallow water models," *Simhydro 2014, Jun 2014, Sophia Antipolis, France*, 2014.

[27] N. Thürey, U. Rüde, and M. Stamminger, "Animation of Open Water Phenomena with coupled Shallow Water and Free Surface Simulations," *Proceedings of the 2006 ACM SIGGRAPH/Eurographics symposium on Computer animation*, pp. 157–164, 2006.

[28] E. Miglio, S. Perotto, and F. Saleri, "Model coupling techniques for free-surface flow problems: Part i," vol. 63, 11 2005.

[29] E. Miglio, S. Perotto, and F. Saleri, "Model coupling techniques for free-surface flow problems: Part II," *Nonlinear Analysis-theory Methods*

& Applications - NONLINEAR ANAL-THEOR METH APP, vol. 63, 2005.

[30] G. Steinebach, S. Rademacher, P. Rentrop, and M. Schulz, "Mechanisms of coupling in river flow simulation systems," *Journal of Computational and Applied Mathematics*, vol. 168, no. 1, pp. 459 – 470, 2004. Selected Papers from the Second International Conference on Advanced Computational Methods in Engineering (ACOMEN 2002).

[31] J. Southard, "Flow in Channels," *Special Topics: An Introduction to Fluid Motions, Sediment Transport, and Current-generated Sedimentary Structures (Lecture Notes)*, pp. 83–156, 2006.

[32] H. Bonakdari, F. Larrarte, L. Lassabatere, and C. Joannis, "Turbulent velocity profile in fully-developed open channel flows," *Environmental Fluid Mechanics*, vol. 8, no. 1, pp. 1–17, 2008.

[33] Q. Zou and X. He, "On pressure and velocity boundary conditions for the lattice Boltzmann BGK model," *Phys. Fluids*, vol. 9, pp. 1591–1598, 1997.

[34] P. Kundu and I. Cohen, *Fluid Mechanics*. Academic Press, 4 ed., 2008.

[35] M. Ben Belgacem, B. Chopard, J. Latt, and A. Parmigiani, "A framework for building a network of irrigation canals on a distributed computing environment: A case study," *Journal of Cellular Automata*, vol. 9, no. 2-3, pp. 225–240, 2014.